MODELLING PRESSURE FLUCTUATIONS DURING FLOW BOILING IN MICROCHANNELS WITH INLET COMPRESSIBILITY AND RESISTANCE

S. Gedupudi, T.G. Karayiannis, D.B.R. Kenning*
Brunel University, Uxbridge, U.K.

ABSTRACT. Confined bubble growth during flow boiling at low pressures in microchannels generates pressure fluctuations that may cause transient flow reversals that disturb the flow distribution in heat sinks formed of parallel channels joined by plena. A simple model is developed for the effects of upstream compressibility and flow resistance at the channel inlet on the magnitude of the pressure transient during the growth of one bubble in a single channel. Preliminary results are presented.

Keywords: *flow boiling, microchannel, heat sink, pressure fluctuations*

INTRODUCTION

Flow boiling at near atmospheric pressure in assemblies of closely-spaced, parallel micro-channels connected by inlet and outlet plena is a promising method of cooling micro-electronic devices at high heat fluxes. The growth of long confined bubbles causes local fluctuations in pressure that may cause temporary reversals of the inlet flow, triggering transient dryout and driving liquid and/or vapour through the plenum towards other channels. The flow reversals may be suppressed by a large frictional resistance at the entry to each channel, e.g. [1-4]. The design guidance is that the time-averaged pressure drop across this resistance should be similar to the pressure drop along the channels. Elimination of flow reversal does not eliminate the pressure fluctuations within channels, which may still influence heat transfer and in extreme cases cause structural damage. Pressure fluctuations have been measured at different axial locations in studies of single channels [5-10] dependent on the compressibility in the upstream boundary conditions, which may result from the pump characteristics or trapped bubbles of vapour or gas. The pressure variations were also measured and simulated by a 1-D model for the special case of bubble growth in an initially uniformly superheated channel with one sealed end (no inlet compressibility, no inlet flow) [11]. 1-D models with different approximations have been developed for oscillatory heat pipes [12].

It is of practical importance to improve the understanding of the effects of bubble-driven pressure fluctuations in assemblies of parallel channels. Parametric studies with 1-D models with simplified physics are less demanding computationally than fully 3-D simulations. A 1-D model for the pressure variations during the growth of a single vapour bubble in a single channel for the special conditions of constant inlet flow (i.e. no inlet compressibility) and constant exit pressure, with features suggested by experimental observations of bubble growth and supported by some 3-D numerical simulations, was presented in [13,14]. The new features of the model, specific to channels of rectangular cross-section of high aspect ratio, are: (i) confinement in two stages, first “partial confinement” by the minor dimension, then “full confinement” by the major dimension of the cross-section, (ii) growth driven by a constant heat flux only to the area of the bubble surface pressed against the heated wall of the channel, Viscous forces are assumed negligible compared to

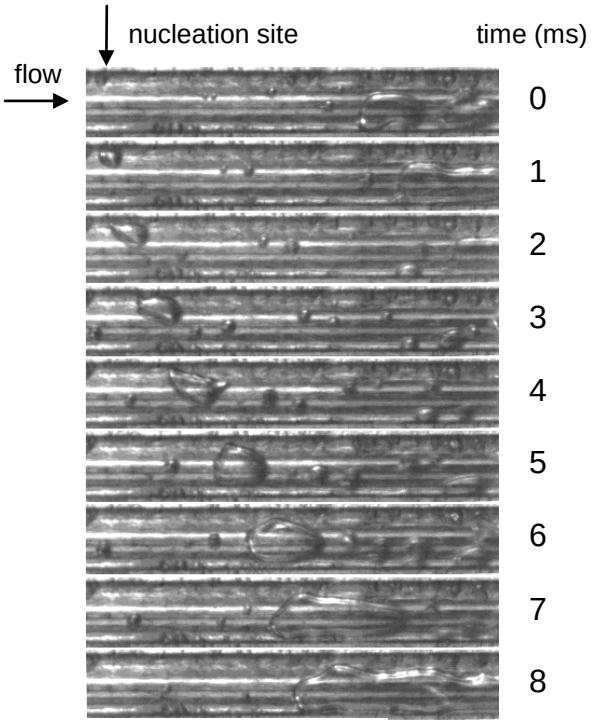

(a) q 219 kW/m^2
U_1 0.7 m/s, ΔT_{sub} 7K

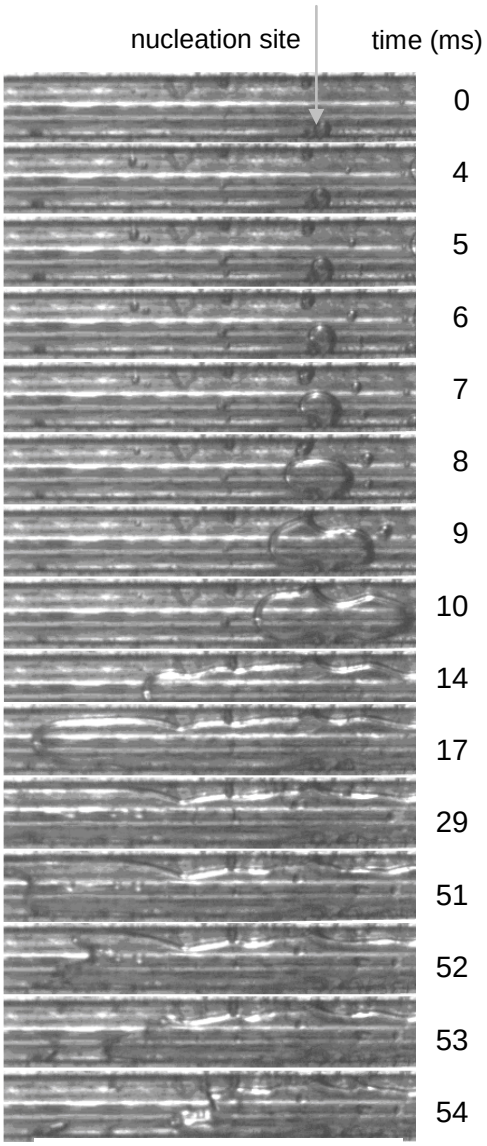

(b) q 173 kW/m^2
U_1 0.7 m/s, ΔT_{sub} 7K

Figure 1. Experimental bubble growth.
(a) No upstream compressibility
(b) With subcooled boiling in preheater

inertial forces. The vapour density is assumed (a) constant, or (b) equal to the saturated vapour density for the instantaneous pressure in the bubble. Variable vapour density is more realistic for the large pressure changes at high heat fluxes and reduces the predicted amplitude of the pressure variations. However, it introduces some modelling problems for a smooth transition to full confinement, discussed in [11] and not yet fully resolved. Using the model with constant vapour density, it was shown that the amplitude of the pressure variation increased with the length of the liquid slug downstream of the bubble nucleation site and with the wall heat flux driving exponential bubble growth.

In this paper, the model for constant density is extended by the addition of sub-models for upstream compressibility in the plenum and a flow resistance at the inlet to the channel. Figure 1 illustrates the sensitivity of bubble motion to apparently minor changes in the rig design that introduced upstream compressibility during experiments on rigorously degassed water boiling at 1.1 bar pressure in a test channel of rectangular section 1.6 mm wide, 0.38 mm deep and 40 mm long, machined in an electrically heated copper block, with a glass window on one side. Reduction in the heat transfer area of the preheater in the external circuit some distance before the test section created compressible vapour due to local subcooled boiling. Further particulars are given in [13].

Examples of bubble growth are shown in Figure 1, (a) with the larger preheater, no upstream compressibility and (b) with subcooled boiling in the smaller preheater creating upstream compressibility despite the same rigorous degassing procedure. In both cases, partial confinement occurred within 2 ms of detectable nucleation but growth to full confinement took 7 - 9 ms. In (a), the growing bubble was pushed downstream by the incoming liquid immediately. Rapid axial

growth only in the downstream direction occurred after full confinement. Nucleation of succeeding bubbles occurred at intervals of about 13 ms, corresponding approximately with the estimated time for the bubble to reach the channel exit. In (b), growth of the partially confined bubble occurred nearly symmetrically in the upstream and downstream directions. Rapid upstream growth occurred after full confinement. The upstream end of the bubble moved out of view at 19 ms and did not return for a further 30 ms. The downstream end of the bubble rapidly moved out of view. The period between nucleation events at the same site was not regular. Recordings at lower magnification showed that more than one nucleation site was active in the channel for both conditions (a) and (b). For images shown in case (a) and (b), nucleation sites were located at about 17mm and 20mm from the inlet respectively.

1-D MODEL FOR CONFINED GROWTH, WITH UPSTREAM COMPRESSIBILITY

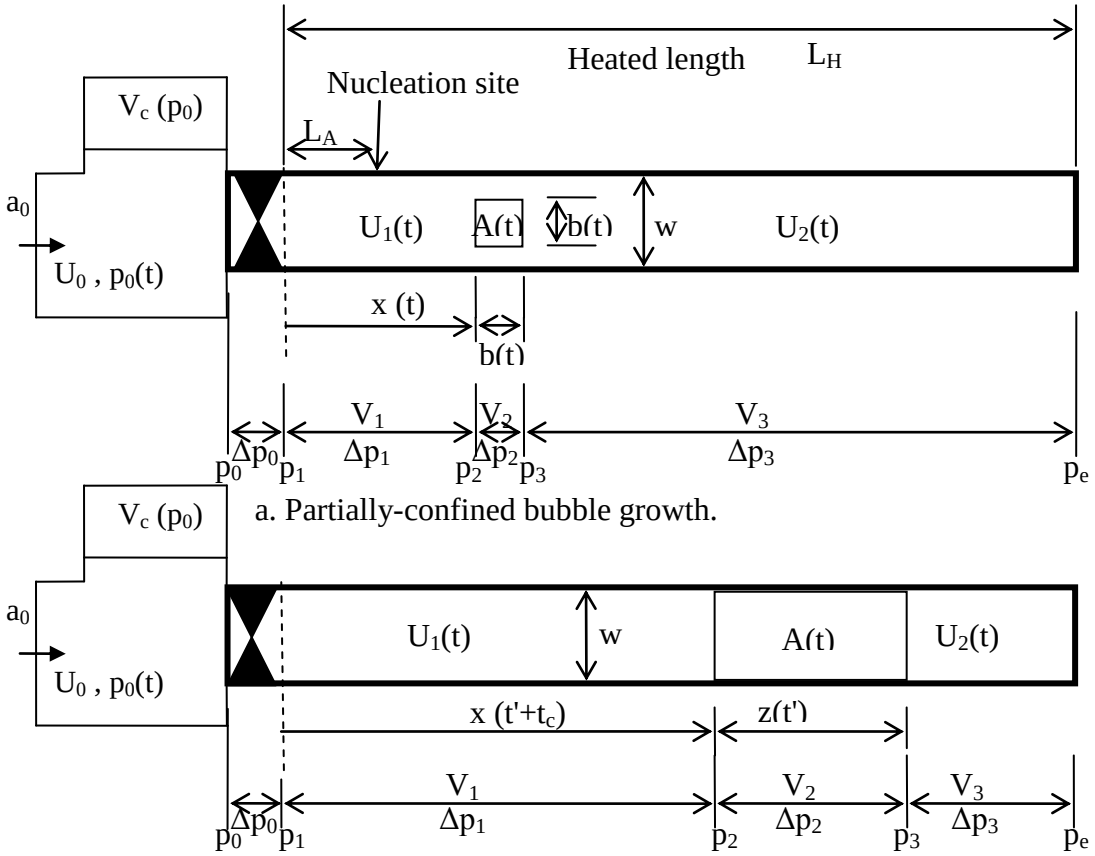

Figure 2. Bubble growth models

The two-stage model for partially and fully confined growth is summarised in Figure 2. The channel is of rectangular section, width w, depth h << w and heated length L_H. Heat input is on one side w with an adiabatic window on the opposite side and negligible heat input on sides h. A single nucleation site is located at L_A from the inlet. A constant volumetric flow rate U_0 a_0 is delivered by the pump to the upstream plenum of cross-sectional area a_0 >> wh so that $p_0(t)$ is the stagnation pressure. A restriction at the channel inlet imposes a frictional resistance with constant loss coefficient F based on the velocity U_1 in the channel so that, depending on the direction of U_1,

$$p_0 - p_1 = [1 + FS(\rho_f/\rho_l)]\,\rho_l\,U_1^2/2, \quad \text{where } S = |U_1| / U_1 \qquad (1)$$

ρ_f depends on whether liquid or vapour phase is passing through the constriction. In the present model, it is assumed that only liquid enters or leaves the upstream end of the channel. Models for flow reversal with vapour passing through the inlet will be developed later.

The plenum is connected to a compressible volume $V_C(t)$ defined by a sub-model, so that

$$(U_0 a_0) + dV_C/dt = whU_1 \qquad (2)$$

Sources of compressibility include presence of vapour or noncondensable gas, connections to parallel channels, pump characteristics, and sub-cooled boiling in the preheater upstream of the channel. In the present model, the only source is assumed to be due to non-condensable gas with initial volume V_{Ci} , as in the Brutin et al. experiments [8]. Assuming an isothermal process,

$$p_0 V_C = p_{0i} V_{Ci}\ ,\ dV_C/dt \ - C\, dp_0/dt, \qquad C = p_{0i} V_{Ci}/p_0^2\ ,\ \approx V_{Ci}/p_e \text{ for small changes} \qquad (3)$$

From (1) – (3),
$$\frac{dp_1}{dt} = \left(\frac{U_0 a_0 - whU_1}{C} \right) - \left(+ FS \rho_l U_1 \frac{dU_1}{dt} \right. \qquad (4)$$

2.1 Partially-confined growth (PC)

The earliest stage of unconfined growth from a nucleus with dimensions << h is neglected. When the bubble is confined fully along the depth h, except for very thin liquid films between the bubble and the surfaces w, it is assumed that the bubble length and width b(t) are equal. Neglecting the volume of the thin liquid films on sides w, the volume of the bubble V(t) is hb^2. Assuming constant heat flux q through the single contact area b^2 and neglecting the change of ρ_v and h_{lv} with pressure,

$$b = he^{t/(2\tau)}\ ,\quad \tau = \rho_v h_{lv} h/q \qquad (5)$$

From continuity,
$$U_2 = U_1 + \left(\right. b^2/w\tau\, e^{t/\tau} \qquad (6)$$

From conservation of momentum, neglecting friction and assuming that the upstream end of the bubble moves at U_1 and the average velocities of the bubble and the liquid alongside are $(U_1+U_2)/2$, the pressure differences over the control volumes V_1, V_2 and V_3, are given by

$$\Delta p_1 = \rho_l \left(U_1 \frac{dx}{dt} + x \frac{dU_1}{dt} \right) + \left(- \rho_l U_1^2 \right) = \rho_l \left(x \frac{dU_1}{dt} \right) \qquad (7)$$

$$\Delta p_2 = \left\{ \left[\left(\rho_l \frac{db}{dt} \right) - \left(\rho_l - \rho_v \right) \frac{2b}{w} \frac{db}{dt} \right] \frac{U_1 + U_2}{2} + \left[\left(\rho_l b \right) - \left(\rho_l - \rho_v \right) \frac{b^2}{w} \right] \frac{1}{2} \left(\frac{dU_1}{dt} + \frac{dU_2}{dt} \right) \right\} \qquad (8)$$

$$\Delta p_3 = \rho_l \left[U_2 \left(- U_1 - \frac{db}{dt} \right) + \left(L_H - x - b \right) \frac{dU_2}{dt} \right] + \left[\rho_l U_2^2 - 0 \right] \qquad (9)$$

From the above equations, with r as the ratio of vapour density to liquid density, ρ_v / ρ_l ,

$$\frac{dU_1}{dt} = \frac{\left(\frac{p_1(t) - p_e}{\rho_l} - U_1 \left[r \frac{h^2}{w\tau} e^{t/\tau} \right] - e^{t/\tau} \frac{h^2}{w\tau^2} (L_H - x) + e^{3t/2\tau} \frac{3h^3}{4w\tau^2} - e^{2t/\tau} \frac{h^4}{w^2\tau^2} r \right)}{\left[L_H - \left(- r \frac{h^2}{w} e^{t/\tau} \right) \right]} \qquad (10)$$

2.2 Fully-confined growth (FC)

Fully-confined bubble growth commences from the time t_c at which b = w. Let $t' = t - t_c$. The contact area A = w z (t'), where z is the length of the bubble, and from the bubble growth equation

$$z = we^{t'/\tau} \qquad (11)$$

From continuity,
$$U_2 = U_1 + \frac{dz}{dt'} = U_1 + \left(\frac{w}{\tau} \right) e^{t'/\tau} \qquad (12)$$

From the momentum equation, assuming that the ends of the bubble move at U_1 and U_2 and its average velocity is $(U_1+U_2)/2$, the pressure differences over the control volumes V_1, V_2 and V_3 are

$$\Delta p_1 = \rho_l \left(U_1 \frac{dx}{dt} + x \frac{dU_1}{dt} \right) + \left(-\rho_l U_1^2 \right) = \rho_l \left(x \frac{dU_1}{dt} \right) \qquad (13)$$

$$\Delta p_2 = \left\{ \left[\left(\rho_v \frac{dz}{dt} \right) \frac{U_1 + U_2}{2} \right] + \left[\rho_v z \frac{1}{2} \left(\frac{dU_1}{dt} + \frac{dU_2}{dt} \right) \right] \right\} + \theta \qquad (14)$$

$$\Delta p_3 = \rho_l \left[U_2 \left(-\frac{dx}{dt} - \frac{dz}{dt} \right) + \left(L_H - x - z \right) \frac{dU_2}{dt} \right] + \left(\rho_l U_2^2 - 0 \right) = \rho_l \left[\left(L_H - x - z \right) \frac{dU_2}{dt} \right] \qquad (15)$$

$$\frac{dU_1}{dt'} = \frac{\left(\frac{p_1(t) - p_e}{\rho_l} - U_1 \frac{rw}{\tau} e^{t'/\tau} - (L_H - x) \frac{w}{\tau^2} e^{t'/\tau} + \left(-r \frac{w^2}{\tau^2} e^{2t'/\tau} \right) \right)}{L_H - \left(-r w e^{t'/\tau} \right)} \qquad (16)$$

The equations are solved by a finite difference method. The incoming flow a_0U_0 and the exit pressure p_e are assumed to be constant. The initial conditions are assumed to be $p_1 = p_e$, $U_1 = a_0U_0 / wh$, neglecting any impulsive changes associated with the initial unconfined growth of the bubble.

SIMULATIONS FOR WATER AT 1 BAR

Conditions

The simulations in this paper correspond to the flow conditions of the visualizations in Figure 1 : water in a channel 0.38 x 1.5 x 40 mm, constant exit pressure of 1 bar, constant inlet flow to the plenum equivalent to a liquid velocity U_1 = 0.7 m/s in the channel. The vapour density is assumed constant and viscous forces are neglected. The nucleation site is placed at the mid-point of the channel, unless otherwise mentioned. At present, the simulation is terminated when either end of a bubble reaches the end of the channel. Simulations for multiple bubbles are under development.

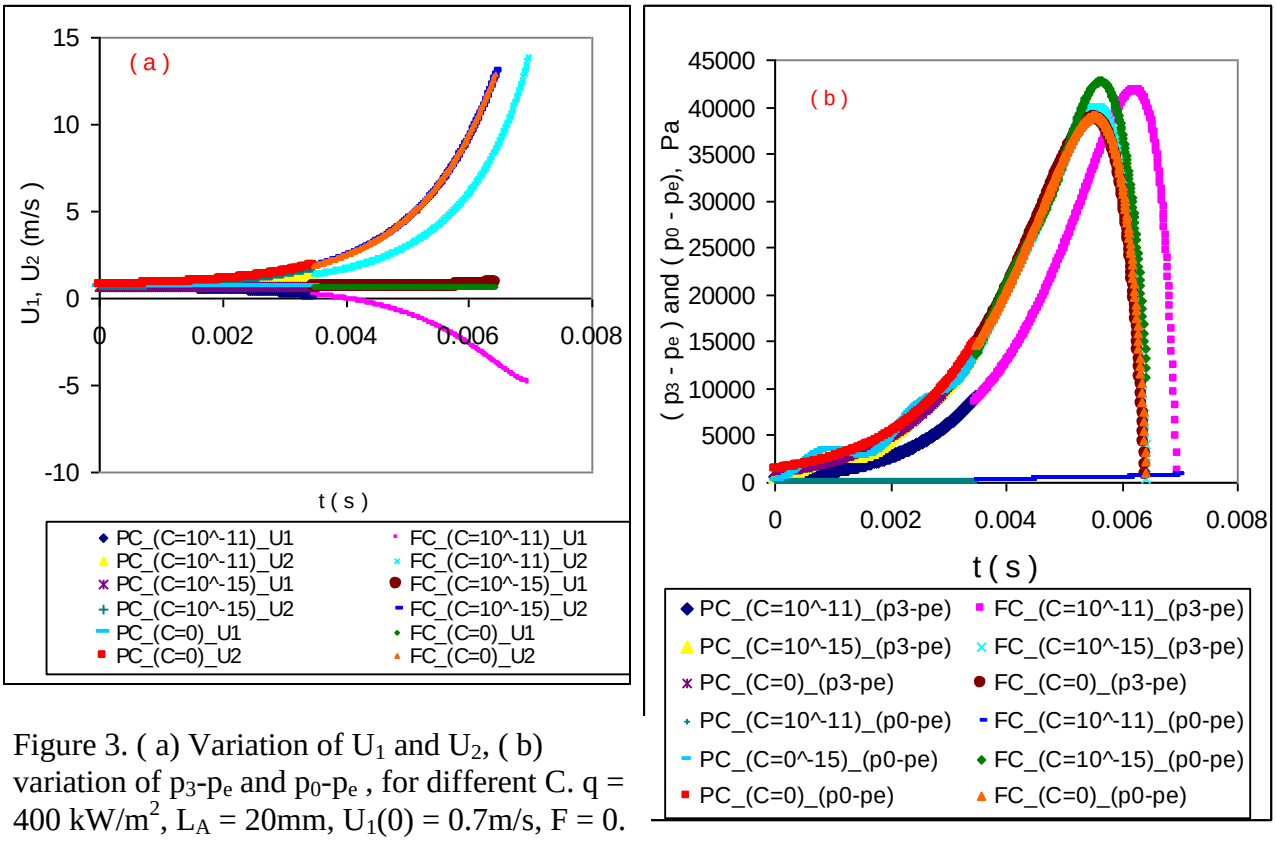

Figure 3. (a) Variation of U_1 and U_2, (b) variation of p_3-p_e and p_0-p_e , for different C. q = 400 kW/m^2, L_A = 20mm, $U_1(0)$ = 0.7m/s, F = 0.

Simulations of the liquid velocities U_1, U_2 on each side of the bubble, the bubble pressure p_3 and the pressure in the inlet plenum p_0 at a heat flux of 400 kW/m^2 are shown in Figure 3 for C = 0, 10^{-11} and 10^{-15}, corresponding respectively to trapped gas volumes in the inlet plenum of 0 (original model in [14]), 1000 mm^3 and 0.1 mm^3 (from Eq.(3)). For comparison, the volume of liquid displaced from the channel to the plenum by movement of one end of the bubble through 20 mm is 11.4 mm^3.

The simulations for C = 10^{-15} are very similar to those for C = 0, except for a small oscillatory component at a frequency of approximately 660 Hz, of the same order as the estimate of 850 Hz for the natural frequency of a spring – mass system using the mass of the upstream liquid column in the channel. The plenum pressure is nearly equal to the bubble pressure. For relatively large upstream compressibility, C = 10^{-11}, the upstream velocity U_1 reverses after about 4 ms , after which growth is nearly symmetrical in the upstream and downstream directions. The bubble pressure rise is reduced and the plenum pressure remains nearly constant. In all the figures, only the total pressure drop ($p_0 - p_e$) and pressure drop at the downstream end of the bubble ($p_3 - p_e$) are shown, and the pressure drop at the upstream end of the bubble ($p_0 - p_3$) can be obtained from it. The pressure drop across the bubble ($p_2 - p_3$) is negligible, at least for the constant vapour property considered in the present model. The simulations show that in the presence of upstream (or inlet) compressibility, the pressure drop at the upstream end will be of the same order of magnitude as that at the downstream end, though they may differ in signs, which makes the total pressure drop between the inlet and outlet much smaller than that for without inlet compressibility. This also shows that for upstream (or inlet) compressibility, the local pressure fluctuations within the channel will be much higher than that between the two channel ends. The amplitude of these pressure fluctuations may be grossly underestimated by experimental measurements of the pressure difference between the inlet and outlet plena.

Additional simulations (not shown here) confirm that the initial asymmetry in growth and the associated delay in flow reversal are modified by changes in the initial incoming flow rate. The amplitude of the bubble pressure within the channel depends strongly on the heat flux, being much smaller at 100 kW/m^2, Figure 4. Also there is no flow reversal for 100 kW/m^2. The simulations performed so far do not exhibit the eventual return of liquid observed in Figure 1(b). Further investigation is required over a wider range of parameters. It may be necessary to use the non-linear version of the compressibility model in Eq.(3), so that the compressibility decreases as reverse flow proceeds, or a different sub-model that is more representative of the subcooled boiling that is the source of compressibility in these particular experiments.

For relatively large compressibility C = 10^{-11}, which maintains the pressure in the inlet plenum nearly constant, a large inlet resistance factor F = 40 reduces the reverse flow into the inlet

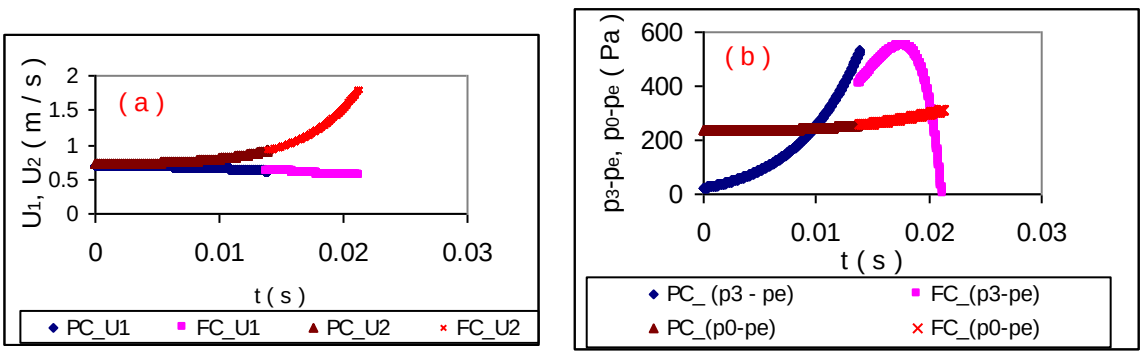

Figure 4. (a) Variation of U_1 and U_2, (b) variation of p_3-p_e and p_0-p_e , for q = 100 kW/m^2, L_A = 20mm, $U_1(0)$ = 0.7m/s and C=10^{-11}, F = 0. Compare with q = 400 kW/m^2 and C=10^{-11} in Figure 3.

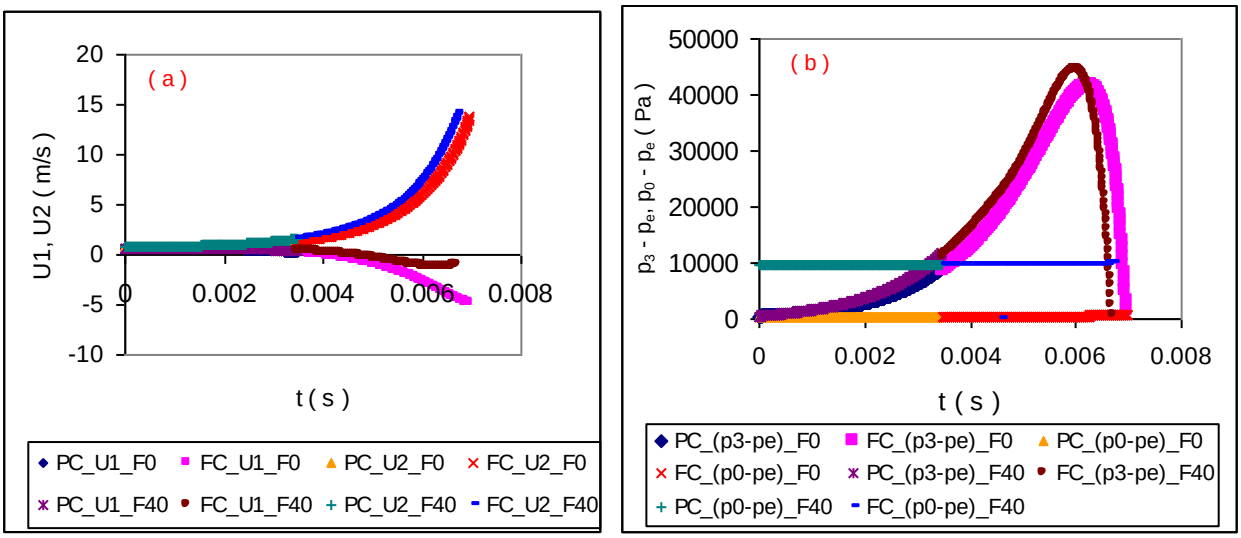

Figure 5. (a) Variation of U_1 and U_2, (b) variation of p_3-p_e and p_0-p_e , for F = 0, 40. q = 400 kW/m^2, L_A = 20mm, $U_1(0)$ = 0.7m/s and C=10^{-11}

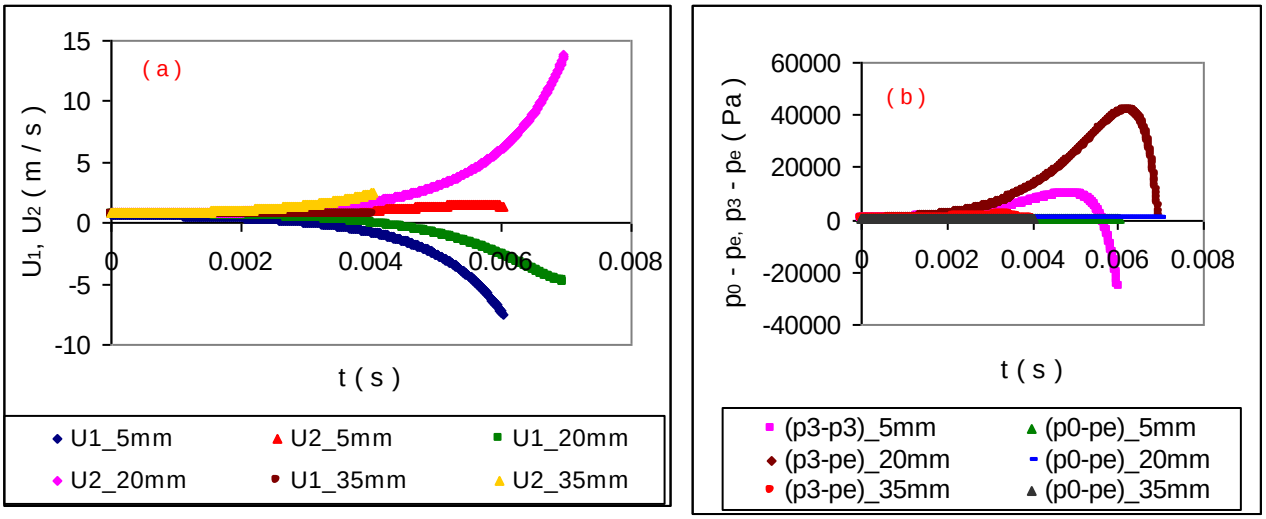

Figure 6. (a)Variation of U_1 and U_2, (b) variation of p_3-p_e and p_0-p_e, for different L_A (5, 20, 35 mm) . q = 400 kW/m^2, L_A = 20mm, U_1 (0) = 0.7 m/s, C=10^{-11}, F=0

plenum but increases slightly the maximum pressure within the channel, Figure 5. Figure 6 shows that the position of the nucleation site influences the reverse flow, with the nucleation site close to inlet showing more flow reversal (negative U_1) than the one at the middle, while the one close to the outlet hardly shows any flow reversal. In the experiments with inlet compressibility, it was observed that the bubbles near the channel inlet and middle grew in both upstream and downstream directions, with irregular periods between nucleation events, whereas those near the outlet only grew in downstream direction with more regular nucleation. The pressure fluctuation ($p_3 - p_e$) caused by the bubble near the outlet is very small compared to that caused by the bubbles near the inlet and middle. However, ($p_0 - p_e$) is very small and similar for all three cases, Figure 6b. The present model considers only single bubble. But in reality, there will be multiple bubbles and their interactions can also influence flow reversal. As the amplitude of pressure fluctuations and their frequencies increase with the heat flux, it will becomes necessary to consider the variation of vapour density and saturation temperature with pressure, not considered in the present bubble growth model.

CONCLUSIONS

A simple model has been developed for the pressure fluctuations and flow reversal caused by the growth of a single vapour bubble in a single micro-channel of rectangular cross-section with upstream compressibility and inlet flow resistance. Preliminary simulations have revealed the interactions between these external influences and conditions within the channel such as the heat flux and the position of the nucleation site. Further development of the model is required to include viscous forces, pressure-dependent vapour properties, different models for compressibility and multiple bubbles that may eventually guide the design of the plena for multichannel heat sinks.

REFERENCES

1. Koşar, A., Kuo, C. J. and Peles, Y., Suppression of boiling flow oscillations in parallel micro-channels by inlet restrictions, *Trans. ASME, J. Heat Transfer*, Vol. 128, pp. 251-260, 2006.
2. Mukherjee, A. and Kandlikar, S.G., Numerical study of the effect of inlet constriction on bubble growth during flow boiling in microchannels, *3rdInternational Conference on Microchannels and Minichannels*, ICMM2005-75143, Toronto, Ontario, Canada, 2005.
3. Kandlikar, S.G., Kuan, W.K., Willistein, D.A. and Borrelli, J., Stabilization of flow boiling in microchannels using pressure drop elements and fabricated nucleation sites, *Trans. ASME, J. Heat Transfer*, Vol. 128, pp. 389-396, 2006.
4. Lee, P.C. and Pan, C., Boiling heat transfer and two-phase flow of water in a single shallow microchannel with a uniform or diverging cross-section, *J. Micromech. Microengineering*, Vol. 18, 025005, 2008.
5. Kenning, D.B.R. and Yan, Y., Saturated flow boiling of water in a narrow channel: experimental investigation of local phenomena, *IChemE Trans. A, Chem. Eng. Research and Design*, Vol. 79, pp. 425-436, 2001.
6. Wen, D.S., Kenning, D.B.R. and Yan, Y., Flow boiling of water in a narrow vertical channel at low mass flux: observations of local phenomena, *Proc.12th Int.Heat Transfer Conf.* Grenoble, Vol. 3, pp. 773-778, 2002.
7. D. Brutin, Topin, F. and Tadrist, L., Experimental study of the unsteady convective boiling in heated minichannels, *Int. J. Heat Mass Transfer*, Vol.46, pp. 2957-2965, 2003.
8. Brutin, D. and Tadrist, L., Pressure drop and heat transfer analysis of flow boiling in a minichannel; influence of the inlet condition on two-phase flow stability, *Int. J. Heat Mass Transfer*, Vol. 47, pp. 2365-2377, 2004.
9. Zhang, L., Goodson, K.E.,and Kenny, T.W., *Silicon Microchannel Heat Sinks,Theories and Phenomena*, Springer Verlag, Berlin, Heidelberg, New York, 2003.
10. Zhang, L., Wang, E.N., Goodson, K.E.,and Kenny, T.W., Phase change phenomena in silicon microchannels, *Int. J. Heat Mass Transfer*, Vol. 48, pp.1572–1582, 2005.
11. Kenning, D.B.R., Wen, D.S., Das, K.S. and Wilson, S.K. Confined growth of a vapour bubble in a capillary tube at initially uniform superheat: experiments and modelling, *Int. J. Heat Mass Transfer*, Vol. 49, pp. 4653-4671, 2006.
12. Shafii, M.B., Faghri, A. and Zhang, Y., Thermal modeling of unlooped and looped pulsating heat pipes, *Trans. ASME, J. Heat Transfer*, Vol. 123, pp. 1159-1172, 2001.
13. Zu, Y.Q., Gedupudi, S., Yan, Y.Y., Karayiannis, T.G. and. Kenning, D.B.R., Numerical simulation and experimental observations of confined bubble growth during flow boiling in a mini-micro channel with a rectangular cross-section of high aspect ratio, *Proc. 7th Int. Conf. on Nanochannels, Microchannels and Minichannels*, paper 82118, Pohang, June 22-24, 2009.
14. Gedupudi, S., Zu, Y.Q., Karayiannis, T.G., Kenning, D.B.R. and Yan, Y.Y., 1-D modelling and 3-D simulation of confined bubble formation and pressure fluctuations during flow boiling in a mini-micro channel with a rectangular cross-section of high aspect ratio, *Proc. 7th Int. Conf. on Nanochannels, Microchannels and Minichannels*, paper 82119, Pohang, June 22-24, 2009.